Supplemental Material for

Stability and Collapse of Holes in Liquid Layers

Cunjing Lv[1,2], Michael Eigenbrod[1], and Steffen Hardt[1*]

[1]*Institute for Nano- and Microfluidics,*

Technische Universität Darmstadt, 64287 Darmstadt, Germany

[2]*Department of Engineering Mechanics,*

Tsinghua University, Beijing 100084, China

(Dated: August 17, 2018)

* hardt@nmf.tu-darmstadt.de
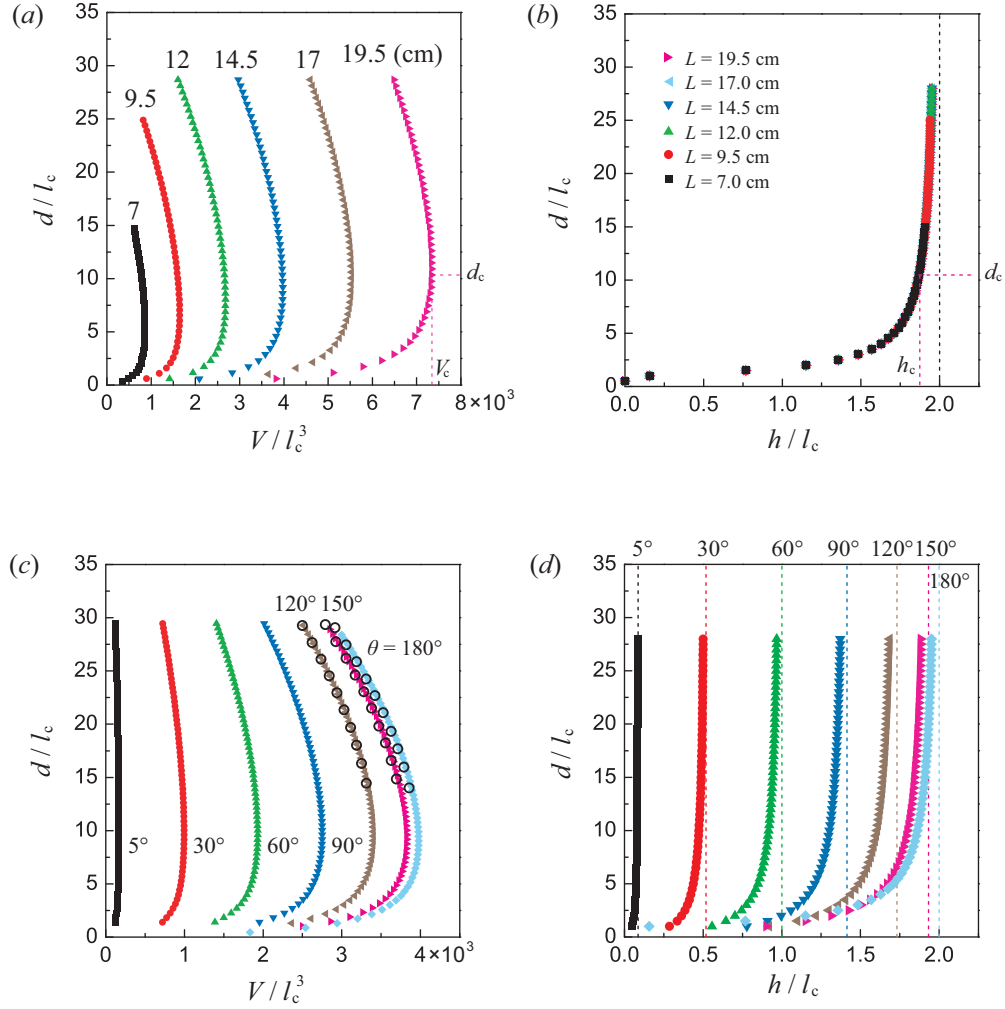
S.1. RELATIONSHIPS OF d VS. V AND d VS. h

FIG. S1. Numerical solution of (3.1) showing the dependence of d on V and of d on h when varying the size of the box and the wettability of the substrate, respectively. (a) and (b) The contact angle is fixed at $\theta = 180°$. Circular boxes with six different diameters L are employed, i.e., $L = 7.0$ cm, 9.5 cm, 12.0 cm, 14.5 cm, 17.0 cm, 19.5 cm. V_c denotes the maximum volume of the liquid, i.e. at the onset of instability. d_c and h_c denote the corresponding hole diameter and the maximum liquid thickness. (c) and (d) The box diameter is fixed at $L = 14.5$ cm, and contact angles of $\theta = 5°$, 30°, 60°, 90°, 120°, 150°, 180° are considered. The black hollow circles are numerical solutions obtained by *Surface Evolver* using a square box with a side length of $L = 14.5$ cm (see Appendix B). The dashed lines in (b) and (d) denote $h = 2l_c \sin(\theta/2)$.

S.2. COMPARISON OF THE EXPERIMENTALLY AND NUMERICALLY OBTAINED LIQUID PROFILES
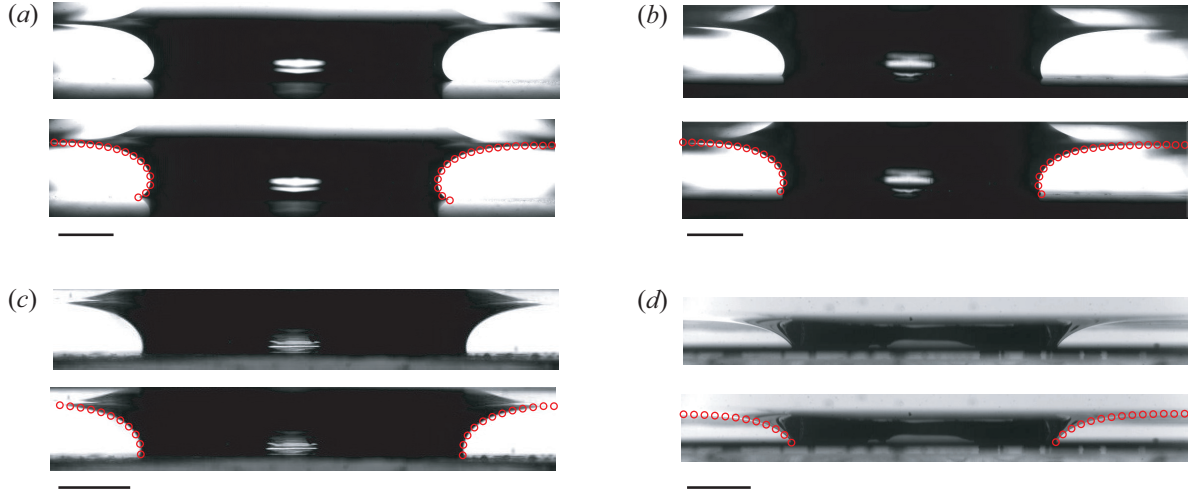

FIG. S2. Comparison of the experimentally and numerically obtained liquid profiles. The numerical data were obtained as described in section 3.1 and are represented as hollow red circles. In each sub-figure, the upper frame is the original experimental image at a certain moment, the lower one shows the comparison. The corresponding substrates and geometrical parameters are: (a) Superhydrophobic Al plate with $\theta_a = 167.5°$, $L = 14.5$ cm, $d = 26.1$ mm; (b) Teflon with $\theta_a = 125.6°$, $L = 14.5$ cm, $d = 24.1$ mm; (c) Liquid-infused glass with $\theta_a = 97.6°$, $L = 14.5$ cm, $d = 23.2$ mm; (d) Silicon wafer with $\theta_a = 55.9°$, $L = 7$ cm, $d = 20.8$ mm. The scale bars represent 5 mm.

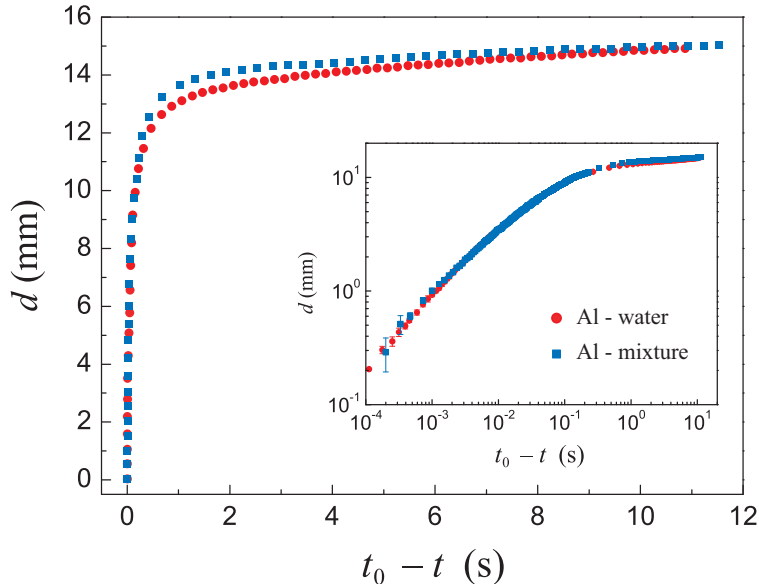## S.3. HOLE COLLAPSE USING LIQUIDS WITH DIFFERENT VISCOSITIES

FIG. S3. Relationship between the instantaneous diameter d of the hole and time $(t_0 - t)$. Two groups of experiments were carried out on Al superhydrophobic substrates with $L = 7$ cm. "Al-water" indicates experiments with water, and "Al-mixture" indicates experiments with water-glycerol mixtures, having a viscosity 2.6 times higher than water. In the main diagram, initially the shrinking of d using water-glycerol mixtures occurs somewhat more slowly than for water, whereas in the final stages of the collapse the two curves are almost identical (see the inset). This demonstrates the weak dependence of the dynamics on the viscosity.

S.4. SIMPLIFIED MODEL FOR THE QUASI-STATIC BEHAVIOR

The numerical results in figure 7 not only show that for all L, d_c slightly decreases with θ, but also show a dependence of d_c on the size of the container. These facts can be qualitatively explained by employing a simplified model, in which it is assumed that the liquid film has a rectangular cross-section, as shown in figure S4. At a certain moment, the volume of the liquid has a specific value. We can write the free energy (which consists of the surface and the gravitational energy) as $E = A_{\mathrm{LV}}\gamma + A_{\mathrm{SL}}(\gamma_{\mathrm{SL}} - \gamma_{\mathrm{LV}}) + \rho V g h/2$. Here $A_{\mathrm{LV}} = \pi[(L/2)^2 - r^2] + 2\pi r h$, $A_{\mathrm{SL}} = \pi[(L/2)^2 - r^2]$, $V = \pi[(L/2)^2 - r^2]h$ and $r = d/2$. We assume that the contact angle between the liquid and the side wall of the container is

$90°$, so we just consider the contribution of A_{SL} from the substrate. However, r (or $h(r)$) is unknown. By minimizing the free energy using $V = $const., we can find r (or $h(r)$).
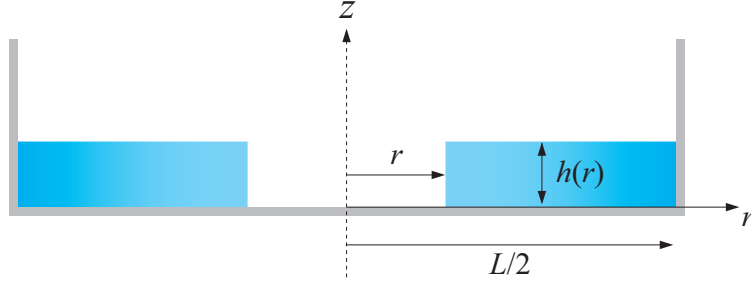

FIG. S4. Sketch of the cross-section of a liquid film with a rectangular shape in a circular container. $r = d(t)/2$ and $h(r)$ are the instantaneous radius and thickness of the liquid film, respectively. L is the diameter of the container.

For convenience, the following calculations are carried out based on dimensionless parameters normalized by the surface tension γ and the capillary length l_{c},

$$\tilde{L} = \frac{L}{l_{\mathrm{c}}}, \quad \tilde{h} = \frac{h}{l_{\mathrm{c}}}, \quad \tilde{r} = \frac{r}{l_{\mathrm{c}}}, \quad \tilde{E} = \frac{E}{l_{\mathrm{c}}^2 \gamma}, \quad \tilde{V} = \frac{V}{l_{\mathrm{c}}^3}. \tag{S1}$$

The free energy $\tilde{E}$ of the system can be written as

$$\tilde{E} = \pi \left[\left(\frac{\tilde{L}}{2} \right)^2 - \tilde{r}^2 \right] \left[\frac{1}{2} \tilde{h}(\tilde{r}) + 1 - \cos\theta \right] + 2\pi \tilde{r} \tilde{h}(\tilde{r}). \tag{S2}$$

From $\partial \tilde{E}/\partial r = 0$, we obtain

$$\tilde{h} = \frac{\tilde{L}^2 + 4\tilde{r}^2 - \sqrt{\tilde{L}^4 + 2\tilde{L}^2(4 + \tilde{L}^2)\tilde{r}^2 - 16(\tilde{L}^2 - 1)\tilde{r}^4 + 32\tilde{r}^6 - 2\tilde{r}^2(\tilde{L}^2 - 4\tilde{r}^2)^2 \cos(\theta)}}{4\tilde{r}^3 - \tilde{L}^2\tilde{r}} \tag{S3}$$

in which we use

$$\frac{\partial \tilde{V}}{\partial \tilde{r}} = 0 \quad \Rightarrow \quad \frac{\partial \tilde{h}}{\partial \tilde{r}} = \frac{2\tilde{r}\tilde{h}}{\left(\frac{\tilde{L}}{2} - \tilde{r}^2 \right)}. \tag{S4}$$

The contact angle θ, which is not represented geometrically in this model, enters indirectly through the interfacial energies. That way, for a system with specific values of the box size L and the contact angle θ, we find r and $h(L)$ for a given volume V. By increasing V and repeating the calculation processes, we can find the minimum value of the hole radius $r_{\mathrm{c}} = r_{\mathrm{min}}$. In figure S5 we plot r_{c} as the function of θ for boxes with different L.
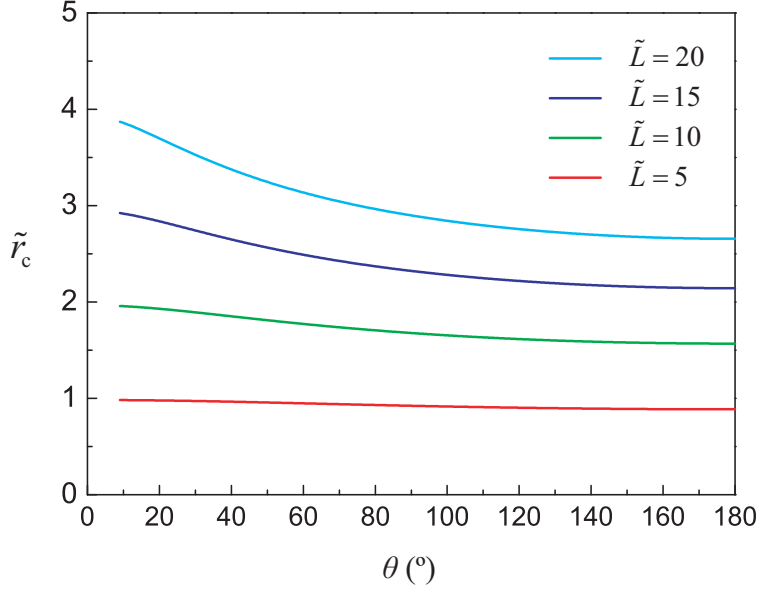
FIG. S5. Results between r_c and θ in dimensionless for containers with different L using the simple model shown in figure S4.

Obviously, this model cannot capture the whole physics of the underlying problem, but shows the same tendency as observed in the numerical solution of the Young-Laplace equation (i.e. figure 7a). For small boxes, the critical radius shows a weak dependence on the contact angle, but for bigger boxes the influence of the contact angle becomes more significant. For a specific value of the contact angle, d_c shows a dependence on the size of the container.

S.5. MOVIE LEGENDS

Supplementary video 1

Hole collapse on a superhydrophobic Al plate viewed from the top. Initially, the hole diameter decreases very slowly when adding more water. The dynamics speed up significantly when d reaches d_c.

Supplementary video 2

Same experiment as in video 1, but captured from the side. This video starts after the onset of instability. After hole collapse, an air bubble is formed on the surface but finally vanishes in the indentations or dissolves.

Supplementary video 3

High-speed video of the final stages of hole collapse in side view (recording speed 100 000 fps).

Supplementary video 4

Hole collapse in a water layer on a Teflon substrate in side view. After the hole is completely closed, there is an air bubble left at the center of the substrate.

Supplementary video 5

Hole collapse on a hydrophilic silicon wafer in side view. Different from the other three samples, here an acute angle at the three-phase contact line is observed. Line pinning is observed in the first stage when the hole is stable. However, beyond the stability threshold the hole collapses rather smoothly.